Structure

Article

Interface refinement of low- to medium-resolution Cryo-EM complexes using HADDOCK2.4

Graphical abstract

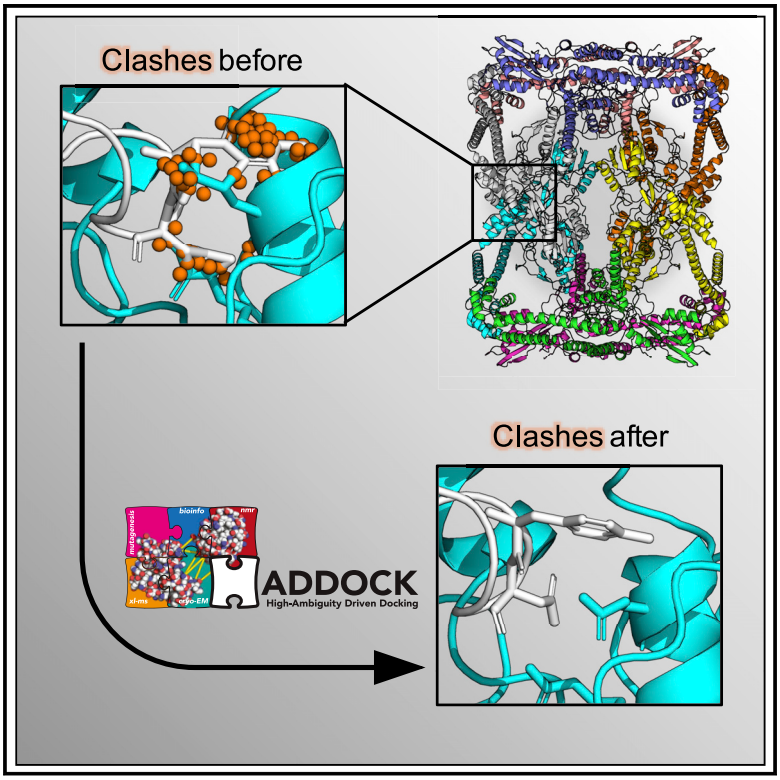

Authors

Tim Neijenhuis, Siri C. van Keulen, Alexandre M.J. J. Bonvin

Correspondence

a.m.j.j.bonvin@uu.nl

In brief

Neijenhuis et al. present an interface refinement protocol to enhance protein-protein interfaces (PPI) of medium-to-low resolution cryo-EM structures using the HADDOCK software package. The protocol leads to a 98% reduction of PPI clashes which results in a more physiologically relevant interface representation.

Highlights

- HADDOCK refinement leads to 98% cryo-EM PPI clash removal
- Cryo-EM interface contact quality is significantly enhanced by HADDOCK refinement
- Structural quality of complexes is best preserved in all-atom refinement protocols

Neijenhuis et al., 2022, Structure *30*, 476–484
April 7, 2022
https://doi.org/10.1016/j.str.2022.02.001

CellPress

CellPress
OPEN ACCESS

Structure

Article

Interface refinement of low- to medium-resolution Cryo-EM complexes using HADDOCK2.4

Tim Neijenhuis,[1] Siri C. van Keulen,[1] and Alexandre M.J. J. Bonvin[1,2,*]
[1]Computational Structural Biology Group, Bijvoet Center for Biomolecular Research, Science for Life, Faculty of Science - Chemistry, Utrecht University, Padualaan 8, 3584 CH, Utrecht, the Netherlands
[2]Lead contact
*Correspondence: a.m.j.j.bonvin@uu.nl
https://doi.org/10.1016/j.str.2022.02.001

SUMMARY

A wide range of cellular processes requires the formation of multimeric protein complexes. The rise of cryo-electron microscopy (cryo-EM) has enabled the structural characterization of these protein assemblies. The density maps produced can, however, still suffer from limited resolution, impeding the process of resolving structures at atomic resolution. In order to solve this issue, monomers can be fitted into low- to medium-resolution maps. Unfortunately, the models produced frequently contain atomic clashes at the protein-protein interfaces (PPIs), as intermolecular interactions are typically not considered during monomer fitting. Here, we present a refinement approach based on HADDOCK2.4 to remove intermolecular clashes and optimize PPIs. A dataset of 14 cryo-EM complexes was used to test eight protocols. The best-performing protocol, consisting of a semi-flexible simulated annealing refinement with centroid restraints on the monomers, was able to decrease intermolecular atomic clashes by 98% without significantly deteriorating the quality of the cryo-EM density fit.

INTRODUCTION

Crucial processes in our cells such as metabolism, signal transduction, gene replication, and transcription all involve an interplay between proteins. Understanding intermolecular interactions in complexes between proteins and other biomolecules is, therefore, key to obtaining a deeper insight into these cellular mechanisms and their potential pathological effects (Arkin and Wells, 2004; Wells and McClendon, 2007). In order to analyze these multimeric protein complexes and their protein-protein interfaces (PPIs), high-quality structures are required. Three common experimental methods to resolve protein structures are X-ray crystallography, nuclear magnetic resonance (NMR), and cryo-electron microscopy (cryo-EM), of which cryo-EM is the experimental method of choice to study large functional complexes (larger than ~80 kDa) (Bai et al., 2015; McPherson and Gavira, 2014). Since the development of direct electron detectors, cryo-EM has become widely used (Bai et al., 2015), which has resulted in a rapid growth of yearly deposited electron density maps (EDMs) (3,827 in 2020) (EMBL-EBI, 2021). The majority of the maps released originate from single-particle (SPA) cryo-EM (77%), yielding an average resolution of 5.6 Å. Other cryo-EM techniques such as tomography, which allows *in situ* detection, cannot yet reach such high resolutions. However, as the *ex situ* conditions of SPA can affect a protein's conformation, the lower-resolution maps obtained with *in situ* techniques are valuable for studying proteins under physiological conditions (Schur, 2019).

De novo modeling of multimeric complexes based on lower-quality electron density maps can be challenging. Often rigid-body fitting of available X-ray/NMR monomeric structures or predicted models (by homology modeling or *in silico* prediction using, e.g., AlphaFold [Jumper et al., 2021] or RoseTTAFold [Baek et al., 2021]) into the EDM is used to build models of those protein complexes (Esquivel-Rodríguez and Kihara, 2013; Malhotra et al., 2019). Various software packages have been developed for this purpose, such as COAN (Volkmann and Hanein, 1999), DOCKEM (Roseman, 2000), EMFIT (Rossmann, 2000), Situs (Wriggers and Birmanns, 2001), UCSF Chimera (Pettersen et al., 2004), Flex-EM (Topf et al., 2008), BLC:EM-Fit (Woetzel et al., 2011), and PowerFit (van Zundert and Bonvin, 2015). After determinination of the initial position of each monomer, the models are often refined with respect to the EDM. An example of such an approach is the refinement of protein models in reciprocal space (e.g., by REFMAC) (Brown et al., 2015; Kovalevskiy et al., 2018). This technique allows the use of well-established methods developed for X-ray crystallography. Other common tools, like phenix.real_space_refine (Adams et al., 2010; Afonine et al., 2018), MDFF/ReMDFF (Singharoy et al., 2016; Trabuco et al., 2008), and Rosetta (Wang et al., 2016), use real-space refinement to optimize models. Rapid developments in the field of protein structure prediction have led to the development of AlphaFold2 and RoseTTAfold, both of which have shown promising results in predicting protein oligo- and heteromeric complexes (Baek et al., 2021; Evans et al., 2021; Yin et al., 2021). In the future, these deep-learning complex models could also

Table 1. Dataset used for interface refinement ordered by number of atomic clashes at the interface

PDB ID	#Clashes[a]	#Chains	#Residues	Resolution(Å)	Probe score/Å^2[b]	PI score[c]	Reference
6R7I	1,053	13	3,911	5.9	−395.95	−0.25	(Faull et al., 2019)
6N1Q	724	8	4,088	5.16	−22.63	0.18	(Soczek et al., 2018)
6UBY	254	9	3,182	7.5	−16.02	0.38	(Huehn et al., 2020)
6N8Z	185	6	5,274	9.3	−67.99	0.08	(Lee et al., 2019)
6IRF	74	4	3,376	5.1	−21.12	1.14	(Zhang et al., 2018)
6UC0	48	8	2,805	7.5	−25.02	1.35	(Huehn et al., 2020)
6AHF	44	6	5,448	6.78	−29.92	0.53	(Zhang et al., 2019)
3J96	36	13	5,988	7.6	−94.39	1.15	(Zhao et al., 2015)
5HNY	24	3	1,235	6.3	−17.20	−0.30	(Yamagishi et al., 2016)
6ACG	21	4	4,212	5.4	−5.59	–	(Song et al., 2018)
5GRS	19	12	3,084	5.4	−52.99	1.30	(Gong et al., 2016)
5WCB	18	6	2,832	6.0	−44.88	0.68	(Zehr et al., 2017)
3J95	15	6	4,482	7.6	−28.25	1.00	(Zhao et al., 2015)
6N7G	7	6	5,744	6.8	−2.73	0.00	(Qian et al., 2019)

[a]Number of intermolecular clashes, defined as heavy atom distances less than 2.5 Å. The average number of clashes over the dataset is 180 ± 315.
[b]Normalized probe score representing the quality of the interface (the larger, more positive, the better), calculated using Molprobity (Word et al., 1999).
[c]Protein interface score was calculated using the PI-score algorithm (Malhotra et al., 2021). The reported values are the average PI-score from the individual interfaces per complex. Model 6ACG was excluded from this analysis due to exceeding the maximum number of atoms that can be analyzed by PI-score.

be used during EDM fitting and PPI refinement, creating a wider range in prediction protocols for large protein assemblies.

Despite the different complex refinement methods, low-resolution cryo-EM models deposited in the PDB often contain a relatively high number of atomic clashes at the PPIs compared with higher-resolution datasets such as the Docking Benchmark 5 (BM5) (Vreven et al., 2015), which includes a low average number of 0.38 ± 0.86 clashes at the interface. These clashes in cryo-EM models are artifacts of the current rigid-body fitting procedure and are often not resolved by refinement, as electrostatics and stereochemical properties might not be fully enforced (Igaev et al., 2019). These clashes contribute to an incorrect or blurry representation of the interfaces in those protein complexes, making it challenging to extract information for further experiments (e.g., mutagenesis) or drug design.

Here, we present a refinement protocol to remove clashes from the PPI of low- to medium-resolution cryo-EM structures using our integrative modeling software package HADDOCK (Dominguez et al., 2003), which has recently been extended to include up to 20 separate molecules per protein complex (Karaca et al., 2017). Eight different protocols are investigated in this study, which are benchmarked on a set of 14 multimeric cryo-EM complexes with resolutions ranging from 5.1 to 9.3 Å. The results show that clashes at the interface of multimeric cryo-EM complexes can be reduced by up to 98% by applying a semi-flexible simulated annealing refinement with restraints on the centroids of the components of the complex without significantly compromising the fit to the EDM.

RESULTS

The 14 multimeric cryo-EM complexes included in our dataset (Table 1; Figure 1) were selected from the PDB based on resolution (in a range of 5 to 10 Å), size (no more than 20 chains) and absence of polynucleotides. These complexes were refined using our integrative modeling software package HADDOCK, version 2.4. A total of eight refinement protocols were tested. In all protocols, the first docking stage, rigid-body docking (it0), was skipped, the complexes were kept in the same orientation as their reference structure, and 50 models were predicted per complex. The first five protocols that were tested use the semi-flexible simulated annealing (SA) stage of HADDOCK (it1) to refine the PPIs. This refinement stage introduces flexibility only in the interfaces and works by performing a series of short molecular dynamics simulations in torsion angle space. Five restraint setups were investigated: No restraints, Cα-Cα atom distance restraints, ambiguous surface restraints, center-of-mass restraints, and centroid restraints. We also tested performing only the final refinement stage (itw), which consists of a short molecular dynamics simulation (MD) in explicit solvent (protocol 6 [(MD]). The last two protocols (protocols 7 [CG] and 8 [CG_MD]) make use of the recent update of HADDOCK supporting coarse graining (CG) (Honorato et al., 2019; Roel-Touris et al., 2019). The last step of this CG docking protocol is the rebuilding of an all-atom (AA) model of the complex. This final CG-to-AA conversion step can also be used as a refinement protocol to remove intermolecular clashes after first converting the models into their CG representation. This was used on both protocols 7 and 8, with the difference that in protocol 8 an additional short MD simulation in explicit solvent was performed. The eight different protocols are summarized in Table 2 and details are provided in the STAR Methods. The performance of the protocols was compared by analyzing the top four models ranked by HADDOCK.

HADDOCK refinement leads to significant PPI clash removal

The first metric we used to assess the performance of the tested refinement protocols was the reduction in the number of

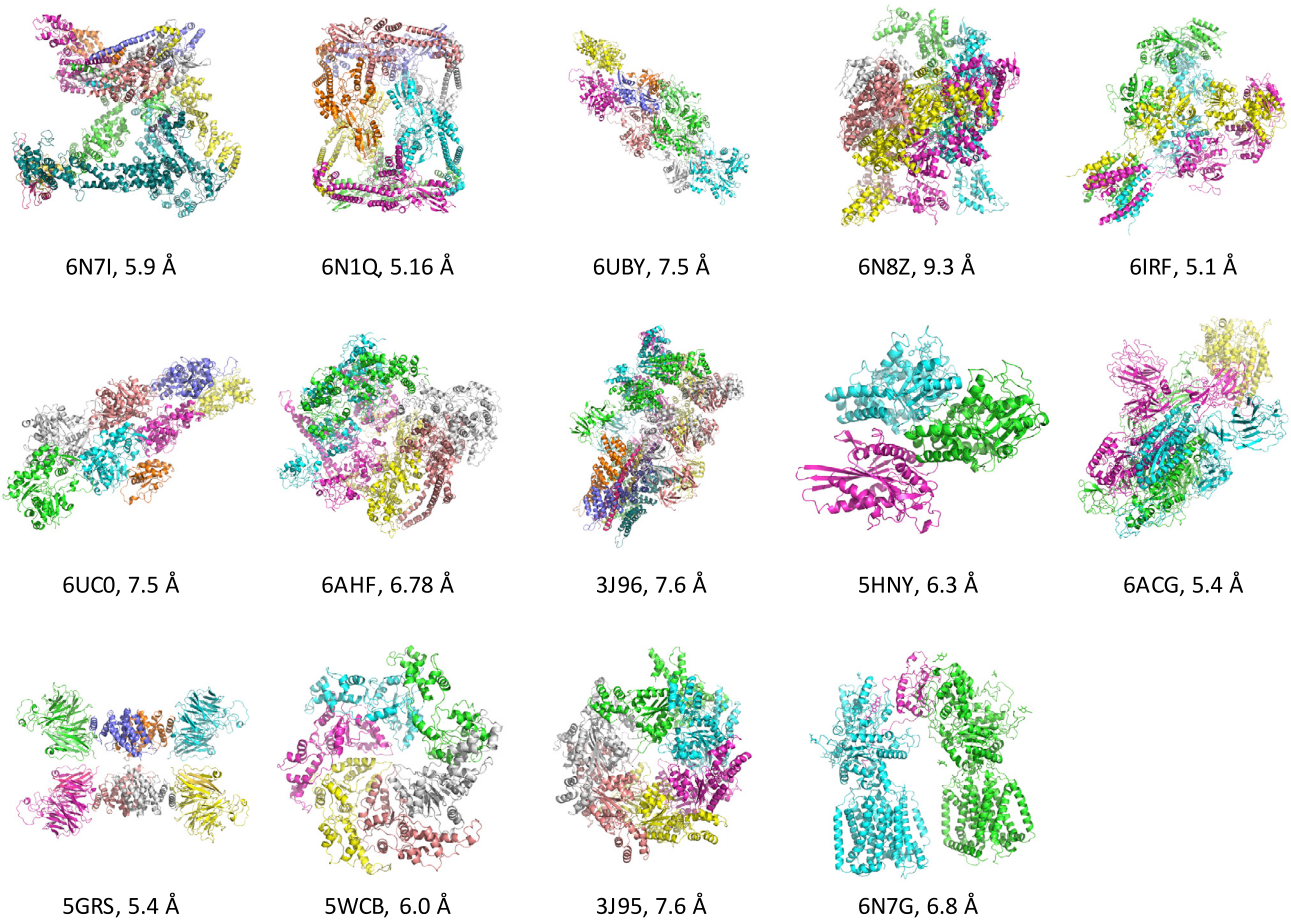

Figure 1. Cartoon representation, PDB IDs and cryo-EM map resolution of the selected 14 cryo-EM complexes. Each protein chain is highlighted by a unique color

interatomic clashes at the PPI. Overall, we observed a significant reduction in the number of clashes with respect to the reference starting structures. All protocols in which simulated annealing was used showed a similar decrease in the number of clashes, from an average of 180 ± 315 in the deposited models (Table 1) to 4 ± 9 in the refined models, corresponding to an average reduction of 98.2% (Figures 2 and 3A). When only a final refinement in explicit solvent was applied to the reference structures (protocol 6: MD), fewer clashes could be removed from the interface. We also observed an increase of interface clashes (from 6 in the reference structure to 27 after MD) for 6N7G, the complex with the lowest number of clashes. The average clash reduction was 63.1%, which was significantly lower than for the annealing protocols. A similar trend was observed for the CG-to-AA conversion refinement protocols, in which the addition of a final refinement in explicit solvent (protocol 8: CG_MD) led to a smaller reduction of intermolecular atomic clashes compared with CG-to-AA conversion alone (protocol 7: CG) (Figure 3A).

CG protocols lead to the best cross-correlation with the EM density

Besides enhancing the quality of the interfaces, the overlap between the cryo-EM electron density map and the refined model also has to be preserved in order for the models to be in line with the experimental data. For each protocol, we calculated the cross-correlation between the refined model and the EM density (CC) and its change with respect to the starting reference structure (Δ_{cc}) (Figure 3B). A positive Δ_{cc} indicates an increase in correlation (improvement of the fit with respect to the EM density), while a negative value indicates a decrease.

Generally, a slight decrease in cross-correlation was observed for all tested protocols (note that the cryo-EM density was not included as a restraint in the refinement). The different types of restraints in the simulated annealing protocols did not result in significantly different Δ_{cc} values, all around −0.01, except for the CM restraints, which led to an average Δ_{cc} of −0.02 ± 0.02. The MD protocol, which included a picosecond timescale MD simulation in explicit solvent, resulted in a similar Δ_{cc} compared with the simulated annealing protocols. The CG-based protocols maintained the best correlation, with Δ_{cc} of −0.005 ± 0.009 and −0.007 ± 0.008, for CG and CG_MD, respectively.

When taking into account only the analysis of the clash removal and density cross-correlation, we can conclude that the CG-to-AA conversion seems to be the best performing refinement method. Additionally, CG also outperforms the other

Table 2. Overview of the tested refinement protocols

Protocol	Method (HADDOCK stage)	Additional restraints	ID
1	Semi-flexible simulated annealing (it1)	–	SA
2	Semi-flexible simulated annealing (it1)	Cα-Cα Distances	SA_CA
3	Semi-flexible simulated annealing (it1)	Surface restraints	SA_SR
4	Semi-flexible simulated annealing (it1)	Center of mass	SA_CM
5	Semi-flexible simulated annealing (it1)	Centroids	SA_CTRD
6	Solvated molecular dynamics (itw)	–	MD
7	Coarse-grained back mapping	–	CG
8	Coarse-grained back mapping and solvated molecular dynamics	–	CG_MD

protocols regarding computational load, requiring the least amount of CPU time of all protocols (Figure S1).

PPI quality is enhanced by HADDOCK refinement

Next, we evaluated the quality of the intermolecular contacts at the PPIs using Probe, which produces an interface score per $Å^2$ (the more positive the score the better the quality of the interface) (Word et al., 1999). The average calculated probe score for the 14 reference complexes of the benchmark was found to be −60 ± 100 (Table 1). All of the tested refinement protocols were able to improve the probe score significantly compared with the reference structures, with average scores ranging between 1.85 and 5.5 (Figure 3C). In line with the clash removal analysis, the protocols including SA produced similar probe scores. Including surface (SA_SR) or centroid (SA_CTRD) restraints resulted in an average score of 5.5, which slightly outperformed the base protocol SA, with an average score of 5.3.

Despite being among the top performing protocols in terms of clash removal and density cross-correlation, interface refinement using CG-to-AA conversion, with (CG_MD) and without (CG), the final water refinement led to an average probe score of 1.8, which was significantly better than the reference complex structures but ranked lowest compared with the other protocols.

Another metric we used to validate the quality of the PPI of the eight proposed protocols is the recently introduced PI score (Malhotra et al., 2021). Here, 12 interface features are calculated ranging from number of interface residues to shape complementary. These features are then used in a support vector machine model, which gives a positive value for predicted native interfaces while giving negative values for predicted non-native interfaces. Hence, the larger the positive score is, the higher is the interface quality.

This analysis was performed on 13 reference complexes of the benchmark (excluding PDB ID 6ACG due to the limitation of maximum number of atoms in the PI-score calculation), resulting in an average PI score of 0.55 ± 0.59 (Table 1). The PI scores of the refined models for the various protocols showed an overall improvement with respect to the reference structures, with average scores per protocol ranging from 1.14 to 1.28 (Figure 3D). The PI scores indicate that the protocols including short MD simulations in explicit solvent (MD and GC_MD) were the lowest-scoring setups, with average scores of 1.14 (still higher than the original structures), whereas the SA protocols resulted in the best-scoring models. Inclusion of Cα (SA_CA) and center-of-mass (SA_CM) restraints led to the best PI scores, with averages of 1.28 and 1.27, respectively. The other SA-based protocols as well as the CG protocol resulted in average scores of 1.23–1.24.

The structural quality of the complete protein complexes is best preserved in all-atom protocols

Since the produced refined structures should maintain their structural integrity while improving the interface quality, we also analyzed the overall structural quality of the produced models. First, we calculated the Ramachandran and rotamer outliers, as well as the Molprobity score and Cα-atom geometries (Davis et al., 2007) for each model. After, the predicted models were checked for the conservation of secondary structure.

Delta values of the Ramachandran outliers with respect to the reference structures are shown in Figure S2A. An increase of Ramachandran outliers, close to 1%, was found for SA-based protocols, whereas outliers remained close to 0 for the MD protocol. The largest number of outliers was detected in the CG protocols (CG and CG_MD). Concerning the rotamer outliers, we observed an increase of more than 11% on average in all five SA protocols (Figure S2B). The rotamer outliers showed a similar trend with respect to the Ramachandran outliers for protocol MD, as fewer rotamer outliers are introduced compared with the simulated annealing protocols. The CG protocol had a similar performance to protocol MD. Protocol CG_MD, however, performed worst of all, with an average increase in rotamer outliers of 14%.

Overall, the Molprobity score, which assesses the structural quality of the entire complex and is dominated by intramolecular components, was slightly increased (indicative of a lower quality) by all protocols compared with the reference structures (Figure S2C). The highest observed score was reached by the CG_MD protocol, with an average score increase of 0.56. All SA-based protocols showed a similar score increase of 0.45, whereas protocols CG and MD showed the least (0.39 and 0.30, respectively). In addition, the delta values of the Cα-atom geometry analysis (Figure S3) indicated that all protocols decreased the overall Cα outlier percentage. The five SA protocols showed similar results, with average delta values of 0.5. The least outlier reduction was observed for the CG protocols, 0.3 and 0.2 on average for CG and CG_MD, respectively.

Finally, for all protocols except the CG refinement, we observed similar secondary structure conservation (Figure S4) with respect to the reference structures. Models from protocol CG included on average a 10% decrease in secondary structure toward the more unstructured turns. Loss of helical structure contributed the most to this secondary structure shift (approximately 9%). The addition of MD simulations (CG_MD) enhanced the number of secondary structure elements. Nonetheless, the

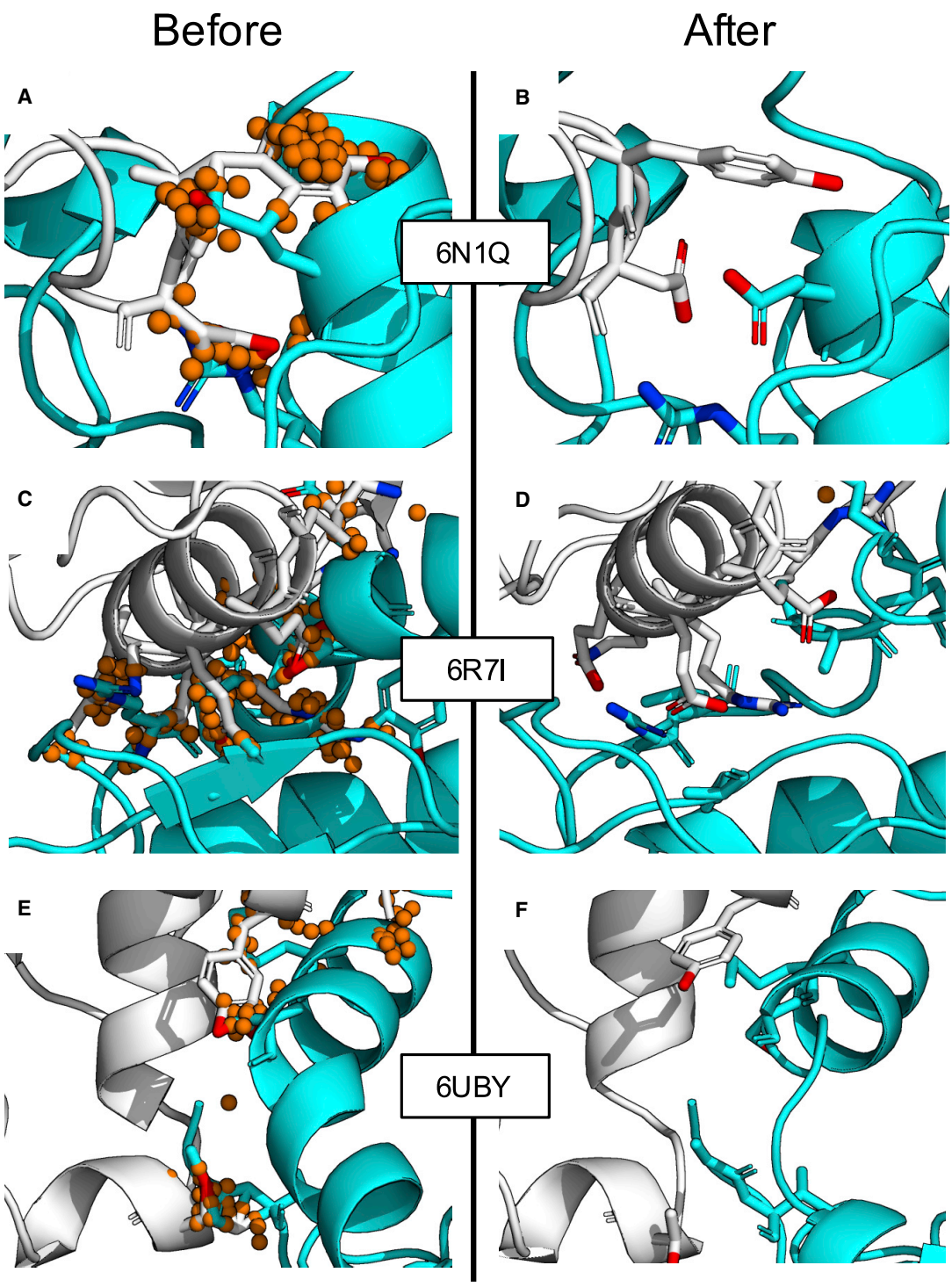

Figure 2. Visualization of intermolecular interactions and atomic clashes at protein-protein interfaces

(A–F) Illustration of intermolecular interactions for interfaces of three presentative complexes (6N1Q, 6R7I, and 6UBY) before (A, C, and E) and after (B, D, and F) clash removal with HADDOCK using protocol 5, the simulated annealing refinement with centroid restraints (SA_CTRD). The orange spheres represent intermolecular clashes (atoms with intermolecular contacts <2.5 Å). Unique protein chains are shown in cyan and gray.

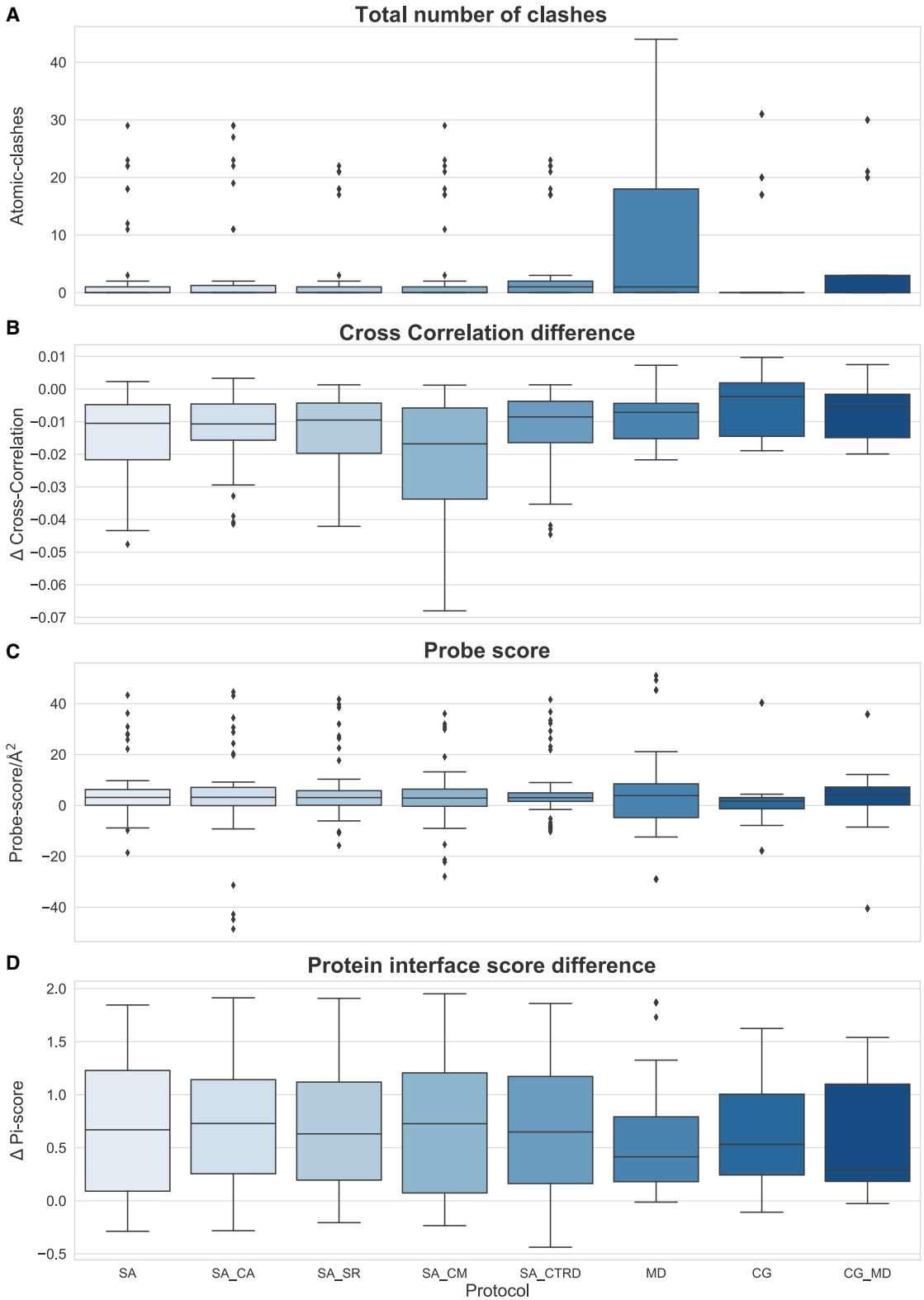

Figure 3. Atomic clashes, probe score, and delta cross-correlation per protocol (Table 2)

Each boxplot includes the top four ranking refined models of all 14 complexes for the corresponding protocol. (A) Number of remaining clashes.

(B) Delta cross-correlation with respect to the reference model (model-reference).

(C) Probe score/Å2.

(D) Delta PI scores (model-reference) for the top four ranking refined models of 13 complexes (higher values indicate more improvement).

(legend continued on next page)

percentage of strands and helices in protocol CG_MD remained significantly lower than for all SA and MD protocols.

It seems that clash removal by CG-to-AA conversion resulted in perturbations of the secondary structure, leading to protein models with larger regions that could not be assigned as standard helix or strand. Although the CG-to-AA back-mapping protocol performed best in clash removal and in maintaining the correlation to the experimental density, it did induce shifts in secondary structure toward less-structured turns conformations.

DISCUSSION

In order to establish which interface refinement approach leads to the highest-quality complex structures of low- to medium-resolution cryo-EM structures, we compared intermolecular clash removal, interface quality, density cross-correlation, backbone quality, and secondary structure conservation. The CaBLAM analysis showed an improvement in overall Cα geometries with respect to the reference structures for all protocols, whereas Molprobity scores were increased for most of the refined complex models, indicating an overall slightly lower quality of the models with respect to the reference structures. The Molprobity score is composed of a log-weighted combination of the clash score, rotamer, and Ramachandran outliers that is calculated over the whole protein complex instead of only considering the PPIs. The increase in Molprobity score for the refined complexes could indicate that resolving the interface clashes comes at the cost of the introduction of less optimal rotamers and backbone configurations. Indeed, PI scores calculated for the refined interface models are improved compared with the reference structures. These findings seem to suggest that, although a slight quality reduction in overall side-chain and backbone configuration is introduced by refinement of the complete complex, the protein interface quality is enhanced by all protocols, making the resulting models more viable to study PPIs.

Because no single protocol scored best for all evaluated features, we assessed the impact of each metric on the overall quality of the refined models to determine the best protocol. All criteria considered, the simulated annealing protocols (1–5) are the best performing in terms of model quality and secondary structure conservation. The top protocol, protocol 5 (SA_CTRD), including centroid restraints, requires minimal prior data generation and leads to enhanced results in density cross-correlation and interface quality, while resulting in similar clash removal compared with the other protocols. Additionally, no secondary structure perturbation is observed with respect to the reference, unrefined structures.

Protocol MD, including solely a short, final refinement via a MD simulation in explicit solvent, performs similarly to protocol SA_CTRD in the delta cross-correlation and secondary structure analysis and even outperforms protocol SA_CTRD in the rotamer and Ramachandran outliers. However, models refined by MD show the highest number of remaining intermolecular clashes, with an average of 8.09 (±13.5). Therefore, this protocol is the least favorable in terms of clash removal, even if on average it decreased the number of clashes by 63.1%. Protocol CG, using CG-to-AA conversion, results in better cross-correlation and PPI clash removal compared with protocol SA_CTRD. CG also shows an increase of cross-correlation for several refined complexes. However, CG also leads to significant secondary structure perturbations (10%). One could argue that secondary structure assignment can be affected by the cutoff used to define a secondary structure element in the employed software. Yet, through manual inspection of the individual complexes, we have observed severe backbone distortions in CG-produced complex structures (data not shown), suggesting that this decrease in secondary structure is not solely a result of the cutoff definition but the result of the effective clash removal. Hence, we deem the CG protocols (protocol CG and CG_MD) less fit to yield accurate interface representations than the other protocols. Therefore, when all metrics are taken into consideration, the SA refinement protocol with centroid restraints (protocol 5, SA_CTRD) appears to be the most optimal protocol to produce realistic PPIs for large protein complexes (see Supplemental information).

CONCLUSION

In this study, we have shown the potential of our integrative docking software HADDOCK for refining the protein-protein interfaces of low- to medium-resolution (5–10 Å) cryo-EM structures of large assemblies. The current version of HADDOCK (version 2.4) allows refinement of complexes including up to 20 subunits, which makes it especially suitable for structural refinement of large multimeric complexes.

After all tested protocols are compared, the protocol including a semi-flexible simulated annealing stage in combination with centroid restraints (SA_CTRD) appears to produce the highest-quality complex structures, removing interatomic clashes by 98% and maintaining the secondary structure of the reference structure. Overall, the models resulting from this refinement approach provide a more realistic representation of the intermolecular interactions than the reference structures, which will facilitate the use of these models to address details of the recognition process and generate new hypotheses such as for residue mutation studies. This refinement protocol has now been implemented in the refinement interface of the HADDOCK2.4 web portal (https://wenmr.science.uu.nl/haddock2.4/refinement), which should facilitate its use. A detailed description on how to run this protocol locally or on the webserver can be found in the Methods S1 and Table S1.

STAR★METHODS

Detailed methods are provided in the online version of this paper and include the following:

- KEY RESOURCES TABLE
- RESOURCE AVAILABILITY
  - Lead contact
  - Materials availability
  - Data and code availability
- EXPERIMENTAL MODEL AND SUBJECT DETAILS
- METHOD DETAILS
  - Data generation and preparation
  - Refinement protocols
- QUANTIFICATION AND STATISTICAL ANALYSIS

SUPPLEMENTAL INFORMATION

Supplemental information can be found online at https://doi.org/10.1016/j.str.2022.02.001

ACKNOWLEDGMENTS

This work was performed with the financial support of the Dutch Foundation for Scientific Research (NWO) (PPS Technology Area grant 741.018.201) and the European Union Horizon 2020 project BioExcel (823830).

AUTHOR CONTRIBUTIONS

Conceptualization, A.B. and S.K.; Methodology, T.N., S.K., and A.B.; Investigation, T.N. and S.K.; Formal Analysis T.N. and S.K.; Data Curation T.N.; Writing – Original Draft T.N., S.K., and A.B.; Writing – Review & Editing T.N., S.K., and A.B.; Funding Acquisition A.B.; Supervision S.K. and A.B.

DECLARATION OF INTERESTS

The authors declare no competing interests.

Received: June 22, 2021
Revised: November 25, 2021
Accepted: January 28, 2022
Published: February 24, 2022

REFERENCES

Adams, P.D., Afonine, P.V., Bunkóczi, G., Chen, V.B., Davis, I.W., Echols, N., Headd, J.J., Hung, L.W., Kapral, G.J., Grosse-Kunstleve, R.W., et al. (2010). PHENIX: a comprehensive Python-based system for macromolecular structure solution. Acta Crystallogr. Sect. D Biol. Crystallogr. *66*, 213–221.

Afonine, P.V., Poon, B.K., Read, R.J., Sobolev, O.V., Terwilliger, T.C., Urzhumtsev, A., and Adams, P.D. (2018). Real-space refinement in PHENIX for cryo-EM and crystallography. Acta Crystallogr. Sect. D Struct. Biol. *74*, 531–544.

Arkin, M.M.R., and Wells, J.A. (2004). Small-molecule inhibitors of protein-protein interactions: progressing towards the dream. Nat. Rev. Drug Discov. *3*, 301–317.

Baek, M., DiMaio, F., Anishchenko, I., Dauparas, J., Ovchinnikov, S., Lee, G.R., Wang, J., Cong, Q., Kinch, L.N., Dustin Schaeffer, R., et al. (2021). Accurate prediction of protein structures and interactions using a three-track neural network. Science *373*, 871–876.

Bai, X., McMullan, G., and Scheres, S.H.W. (2015). How cryo-EM is revolutionizing structural biology. Trends Biochem. Sci. *40*, 49–57.

Brown, A., Long, F., Nicholls, R.A., Toots, J., Emsley, P., and Murshudov, G. (2015). Tools for macromolecular model building and refinement into electron cryo-microscopy reconstructions. Acta Crystallogr. Sect. D Biol. Crystallogr. *71*, 136–153.

Davis, I.W., Leaver-Fay, A., Chen, V.B., Block, J.N., Kapral, G.J., Wang, X., Murray, L.W., Arendall, W.B., Snoeyink, J., Richardson, J.S., et al. (2007). MolProbity: all-atom contacts and structure validation for proteins and nucleic acids. Nucleic Acids Res. *35*, 375–383.

Dominguez, C., Boelens, R., and Bonvin, A.M.J.J. (2003). HADDOCK: a protein-protein docking approach based on biochemical or biophysical information. J. Am. Chem. Soc. *125*, 1731–1737.

EMBL-EBI (2021). Electron Microscopy Data Base Statistics.

Esquivel-Rodríguez, J., and Kihara, D. (2013). Computational methods for constructing protein structure models from 3D electron microscopy maps. J. Struct. Biol. *184*, 93–102.

Evans, R., O'Neill, M., Pritzel, A., Antropova, N., Senior, A., Green, T., Žídek, A., Bates, R., Blackwell, S., Yim, J., et al. (2021). Protein complex prediction with alphafold-multimer. BioRxiv.

Faull, S.V., Lau, A.M.C., Martens, C., Ahdash, Z., Hansen, K., Yebenes, H., Schmidt, C., Beuron, F., Cronin, N.B., Morris, E.P., et al. (2019). Structural basis of Cullin 2 RING E3 ligase regulation by the COP9 signalosome. Nat. Commun. *10*, 1–13.

Frishman, D., and Argos, P. (1995). Knowledge-based protein secondary structure assignment. Proteins Struct. Funct. Bioinforma. *23*, 566–579.

Gong, X., Qian, H., Shao, W., Li, J., Wu, J., Liu, J.J., Li, W., Wang, H.W., Espenshade, P., and Yan, N. (2016). Complex structure of the fission yeast SREBP-SCAP binding domains reveals an oligomeric organization. Cell Res. *26*, 1197–1211.

Hintze, B.J., Lewis, S.M., Richardson, J.S., and Richardson, D.C. (2016). Molprobity's ultimate rotamer-library distributions for model validation. Proteins Struct. Funct. Bioinforma. *84*, 1177–1189.

Honorato, R.V., Roel-Touris, J., and Bonvin, A.M.J.J. (2019). MARTINI-based protein-DNA coarse-grained HADDOCKing. Front. Mol. Biosci. *6*, 1–8.

Huehn, A.R., Bibeau, J.P., Schramm, A.C., Cao, W., De La Cruz, E.M., and Sindelar, C.V. (2020). Structures of cofilin-induced structural changes reveal local and asymmetric perturbations of actin filaments. Proc. Natl. Acad. Sci. U S A *117*, 1478–1484.

Igaev, M., Kutzner, C., Bock, L.V., Vaiana, A.C., and Grubmüller, H. (2019). Automated cryo-EM structure refinement using correlation-driven molecular dynamics. Elife *8*, 1–33.

Jiménez-García, B., Roel-Touris, J., Romero-Durana, M., Vidal, M., Jiménez-González, D., and Fernández-Recio, J. (2018). LightDock: a new multi-scale approach to protein-protein docking. Bioinformatics *34*, 49–55.

Jumper, J., Evans, R., Pritzel, A., Green, T., Figurnov, M., Ronneberger, O., Tunyasuvunakool, K., Bates, R., Žídek, A., Potapenko, A., et al. (2021). Highly accurate protein structure prediction with AlphaFold. Nature *596*, 583–589.

Karaca, E., Rodrigues, J.P.G.L.M., Graziadei, A., Bonvin, A.M.J.J., and Carlomagno, T. (2017). M3: an integrative framework for structure determination of molecular machines. Nat. Methods *14*, 897–902.

Kovalevskiy, O., Nicholls, R.A., Long, F., Carlon, A., and Murshudov, G.N. (2018). Overview of refinement procedures within REFMAC 5: utilizing data from different sources. Acta Crystallogr. Sect. D Struct. Biol. *74*, 215–227.

Lee, S., Roh, S.H., Lee, J., Sung, N., Liu, J., and Tsai, F.T.F. (2019). Cryo-EM structures of the Hsp104 protein disaggregase captured in the ATP conformation. Cell Rep. *26*, 29–36.e3.

Malhotra, S., Träger, S., Dal Peraro, M., and Topf, M. (2019). Modelling structures in cryo-EM maps. Curr. Opin. Struct. Biol. *58*, 105–114.

Malhotra, S., Joseph, A.P., Thiyagalingam, J., and Topf, M. (2021). Assessment of protein–protein interfaces in cryo-EM derived assemblies. Nat. Commun. *12*, 1–12.

McPherson, A., and Gavira, J.A. (2014). Introduction to protein crystallization. Acta Crystallogr F Struct Biol Commun *70*, 2–20.

Monticelli, L., Kandasamy, S.K., Periole, X., Larson, R.G., Tieleman, D.P., and Marrink, S.J. (2008). The MARTINI coarse-grained force field: extension to proteins. J. Chem. Theor. Comput. *4*, 819–834.

Pettersen, E.F., Goddard, T.D., Huang, C.C., Couch, G.S., Greenblatt, D.M., Meng, E.C., and Ferrin, T.E. (2004). UCSF Chimera - a visualization system for exploratory research and analysis. J. Comput. Chem. *25*, 1605–1612.

Prisant, M.G., Williams, C.J., Chen, V.B., Richardson, J.S., and Richardson, D.C. (2020). New tools in MolProbity validation: CaBLAM for CryoEM backbone, UnDowser to rethink "waters," and NGL Viewer to recapture online 3D graphics. Protein Sci. *29*, 315–329.

Qian, H., Cao, P., Hu, M., Gao, S., Yan, N., and Gong, X. (2019). Inhibition of tetrameric patched1 by sonic hedgehog through an asymmetric paradigm. Nat. Commun. *10*, 1–9.

Rodrigues, J.P.G.L.M., Teixeira, J.M.C., Trellet, M., and Bonvin, A.M.J.J. (2018). Pdb-tools: a swiss army knife for molecular structures [version 1; referees: 2 approved]. F1000Res. *7*, 1–8.

Roel-Touris, J., Don, C.G., Honorato, R.R., Rodrigues, J.P.G.L.M., and Bonvin, A.M.J.J. (2019). Less is more: coarse-grained integrative modeling of large biomolecular assemblies with HADDOCK. J. Chem. Theor. Comput. *15*, 6358–6367.

Roel-Touris, J., Jiménez-García, B., and Bonvin, A.M.J.J. (2020). Integrative modeling of membrane-associated protein assemblies. Nat. Commun. *11*, 1–11.

Roseman, A.M. (2000). Docking structures of domains into maps from cryo-electron microscopy using local correlation. Acta Crystallogr. Sect. D Biol. Crystallogr. *56*, 1332–1340.

Rossmann, M.G. (2000). Fitting atomic models into electron-microscopy maps. Acta Crystallogr. Sect. D Biol. Crystallogr. *56*, 1341–1349.

Schrodinger, L.L.C. (2015). The PyMOL Molecular Graphics System, Version 1.8 (Schrödinger).

Schur, F.K. (2019). Toward high-resolution in situ structural biology with cryo-electron tomography and subtomogram averaging. Curr. Opin. Struct. Biol. *58*, 1–9.

Singharoy, A., Teo, I., McGreevy, R., Stone, J.E., Zhao, J., and Schulten, K. (2016). Molecular dynamics-based refinement and validation for sub-5 Å cryo-electron microscopy maps. Elife *5*, 1–33.

Soczek, K.M., Grant, T., Rosenthal, P.B., and Mondragón, A. (2018). CryoEM structures of open dimers of gyrase A in complex with DNA illuminate mechanism of strand passage. Elife *7*, 1–23.

Song, W., Gui, M., Wang, X., and Xiang, Y. (2018). Cryo-EM structure of the SARS coronavirus spike glycoprotein in complex with its host cell receptor ACE2. PLoS Pathog. *14*, 1–19.

Topf, M., Lasker, K., Webb, B., Wolfson, H., Chiu, W., and Sali, A. (2008). Protein structure fitting and refinement guided by Cryo-EM density. Structure *16*, 295–307.

Trabuco, L.G., Villa, E., Mitra, K., Frank, J., and Schulten, K. (2008). Flexible fitting of atomic structures into electron microscopy maps using molecular dynamics. Structure *16*, 673–683.

Volkmann, N., and Hanein, D. (1999). Quantitative fitting of atomic models into observed densities derived by electron microscopy. J. Struct. Biol. *125*, 176–184.

Vreven, T., Moal, I.H., Vangone, A., Pierce, B.G., Kastritis, P.L., Torchala, M., Chaleil, R., Jiménez-García, B., Bates, P.A., Fernandez-Recio, J., et al. (2015). Updates to the integrated protein-protein interaction benchmarks: docking benchmark version 5 and affinity benchmark version 2. J. Mol. Biol. *427*, 3031–3041.

Wang, R.Y.R., Song, Y., Barad, B.A., Cheng, Y., Fraser, J.S., and DiMaio, F. (2016). Automated structure refinement of macromolecular assemblies from cryo-EM maps using Rosetta. Elife *5*, 1–22.

Wells, J.A., and McClendon, C.L. (2007). Reaching for high-hanging fruit in drug discovery at protein-protein interfaces. Nature *450*, 1001–1009.

Williams, C.J., Headd, J.J., Moriarty, N.W., Prisant, M.G., Videau, L.L., Deis, L.N., Verma, V., Keedy, D.A., Hintze, B.J., Chen, V.B., et al. (2018). MolProbity: more and better reference data for improved all-atom structure validation. Protein Sci. *27*, 293–315.

Woetzel, N., Lindert, S., Stewart, P.L., and Meiler, J. (2011). BCL::EM-Fit: rigid body fitting of atomic structures into density maps using geometric hashing and real space refinement. J. Struct. Biol. *175*, 264–276.

Word, J.M., Lovell, S.C., Labean, T.H., Taylor, H.C., Zalis, M.E., Presley, B.K., Richardson, J.S., and Richardson, D.C. (1999). Visualizing and quantifying molecular goodness-of-fit: small-probe contact dots with explicit hydrogen atoms. J. Mol. Biol. *285*, 1711–1733.

Wriggers, W., and Birmanns, S. (2001). Using situs for flexible and rigid-body fitting of multiresolution single-molecule data. J. Struct. Biol. *133*, 193–202.

Yamagishi, M., Shigematsu, H., Yokoyama, T., Kikkawa, M., Sugawa, M., Aoki, M., Shirouzu, M., Yajima, J., and Nitta, R. (2016). Structural basis of backwards motion in kinesin-1-kinesin-14 chimera: implication for kinesin-14 motility. Structure *24*, 1322–1334.

Yin, R., Feng, B.Y., Varshney, A., and Pierce, B.G. (2021). Benchmarking AlphaFold for protein complex modeling reveals accuracy determinants. BioRxiv.

Zehr, E., Szyk, A., Piszczek, G., Szczesna, E., Zuo, X., and Roll-Mecak, A. (2017). Katanin spiral and ring structures shed light on power stroke for microtubule severing. Nat. Struct. Mol. Biol. *24*, 717–725.

Zhang, J.B., Chang, S., Xu, P., Miao, M., Wu, H., Zhang, Y., Zhang, T., Wang, H., Zhang, J., Xie, C., et al. (2018). Structural basis of the proton sensitivity of human GluN1-GluN2A NMDA receptors. Cell Rep. *25*, 3582–3590.e4.

Zhang, X., Zhang, S., Zhang, L., Lu, J., Zhao, C., Luo, F., Li, D., Li, X., and Liu, C. (2019). Heat shock protein 104 (HSP104) chaperones soluble Tau via a mechanism distinct from its disaggregase activity. J. Biol. Chem. *294*, 4956–4965.

Zhao, M., Wu, S., Zhou, Q., Vivona, S., Cipriano, D.J., Cheng, Y., and Brunger, A.T. (2015). Mechanistic insights into the recycling machine of the SNARE complex. Nature *518*, 61–67.

van Zundert, G.C.P., and Bonvin, A.M.J.J. (2015). Fast and sensitive rigid-body fitting into cryo-EM density maps with PowerFit. AIMS Biophys. *2*, 73–87.

Van Zundert, G.C.P., Rodrigues, J.P.G.L.M., Trellet, M., Schmitz, C., Kastritis, P.L., Karaca, E., Melquiond, A.S.J., Van Dijk, M., De Vries, S.J., and Bonvin, A.M.J.J. (2016). The HADDOCK2.2 web server: user-friendly integrative modeling of biomolecular complexes. J. Mol. Biol. *428*, 720–725.

STAR★METHODS

KEY RESOURCES TABLE

REAGENT or RESOURCE	SOURCE	IDENTIFIER
Deposited data		
Raw and analyzed data	This paper	https://doi.org/10.5281/zenodo.5832624
PDB ID: 6R7I (EMD-4742)	(Faull et al., 2019)	https://dx.doi.org/10.2210/pdb6r71/pdb
PDB ID: 6N1Q (EMD-9317)	(Soczek et al., 2018)	https://dx.doi.org/10.2210/pdb6n1q/pdb
PDB ID: 6UBY (EMD-20721)	(Huehn et al., 2020)	https://dx.doi.org/10.2210/pdb6uby/pdb
PDB ID: 6N8Z (EMD-0377)	(Lee et al., 2019)	https://dx.doi.org/10.2210/pdb6n8z/pdb
PDB ID: 6IRF (EMD-9715)	(Zhang et al., 2018)	https://dx.doi.org/10.2210/pdb6n8z/pdb
PDB ID: 6UC0 (EMD-20724)	(Huehn et al., 2020)	https://dx.doi.org/10.2210/pdb6uc0/pdb
PDB ID: 6AHF (EMD-9625)	(Zhang et al., 2019)	https://dx.doi.org/10.2210/pdb6ahf/pdb
PDB ID: 3J96 (EMD-6206)	(Zhao et al., 2015)	https://dx.doi.org/10.2210/pdb6ahf/pdb
PDB ID: 5HNY (EMD-8060)	(Yamagishi et al., 2016)	https://dx.doi.org/10.2210/pdb5hny/pdb
PDB ID: 6ACG (EMD-9591)	(Song et al., 2018)	https://dx.doi.org/10.2210/pdb6acg/pdb
PDB ID: 5GRS (EMD-9537)	(Gong et al., 2016)	https://dx.doi.org/10.2210/pdb5grs/pdb
PDB ID: 5WCB (EMD-8796)	(Zehr et al., 2017)	https://dx.doi.org/10.2210/pdb5wcb/pdb
PDB ID: 3J95 (EMD-6205)	(Zhao et al., 2015)	https://dx.doi.org/10.2210/pdb3j96/pdb
PDB ID: 6N7G (EMD-0355)	(Qian et al., 2019)	https://dx.doi.org/10.2210/pdb6n7g/pdb
Software and algorithms		
HADDOCK	(Dominguez et al., 2003),	https://wenmr.science.uu.nl/haddock2.4/
PDB-Tools	(Rodrigues et al., 2018)	https://wenmr.science.uu.nl/pdbtools/
UCSF Chimera	(Pettersen et al., 2004)	https://www.cgl.ucsf.edu/chimera/
Molprobity	(Davis et al., 2007; Prisant et al., 2020)	http://molprobity.biochem.duke.edu
PI score	(Malhotra et al., 2021)	https://gitlab.com/topf-lab/pi_score
STRIDE	Frishman and Argos, 1995)	http://webclu.bio.wzw.tum.de/stride/
PyMOL	(Schrodinger, 2015)	https://pymol.org/2/

RESOURCE AVAILABILITY

Lead contact

Further information and requests for resources should be directed to and will be fulfilled by the Lead Contact Alexandre M.J.J. Bonvin (a.m.j.j.bonvin@uu.nl)

Materials availability

This study did not generate new unique reagents.

Data and code availability

This paper analyzes existing, publicly available data. These accession numbers for the datasets are listed in the key resources table (KRT). All original code has been deposited at https://github.com/haddocking/refine-EM-complexes (https://dx.doi.org/10.5281/zenodo.5832624) and are publicly available as of the date of publication. DOIs are listed in the KRT. Any additional information required to reanalyze the data reported in this paper is available from the lead contact upon request.

EXPERIMENTAL MODEL AND SUBJECT DETAILS

All data are generated from the dataset provided in the KRT.

METHOD DETAILS

Data generation and preparation

The dataset used to benchmark the protocols described in this work is composed of 14 cryo-EM complexes in a resolution range of 5–10 Å. Complexes were selected based on the following criteria: (i) a chain count of up to 20, (ii) absence of nucleic acids and (iii)

minimal redundancy within the dataset. The fourteen complexes selected are summarized in Table 1 and visualized in Figure 1. The structures were prepared using pdb-tools (Rodrigues et al., 2018). Co-factors distant from any interface were removed for convenience using PDB_delresname.py and noncanonical amino acids were substituted for their canonical counterparts using PDB_rplresname.py (e.g. MSE to MET). The individual chains were finalized for use in HADDOCK using PDB_tidy.py.

Refinement protocols

We used our integrative modeling software package HADDOCK, version 2.4, to refine the protein complexes in the dataset, testing several protocols to remove atomic clashes at the interfaces of these multimeric protein complexes. The default HADDOCK protocol consists of three stages. First, rigid body docking (it0) is performed in which each protein is treated as a rigid entity (Dominguez et al., 2003). This docking step is usually guided by experimental or predicted interaction information, translated into distance restraints which bias specific protein regions to interact without predefining their relative orientation. Subsequently, the best models from it0 (200 by default) move to stage two (it1), which refines the PPIs via simulated annealing protocol in torsion angle space. Here, flexibility is gradually added to the protein interface, first for side chains and then both side chains and backbone, to allow for small conformational changes and optimize the intermolecular interactions. The third and last stage consists of a final refinement (itw). In this step, the protein-protein interface is refined by either an energy minimization (default in HADDOCK2.4) or by a very short molecular dynamics simulation using an explicit solvent shell. Eight different refinement protocols were considered in this work (Table 2). In all cases the rigid body docking stage (it0) was skipped and the complexes were kept in their original orientation (randomization of starting orientations turned off). For all protocols, the number of models to be generated was set to 50 for all stages of HADDOCK.

Semi-flexible interface refinement (protocols 1–5)

The first five protocols use the semi-flexible simulated annealing stage of HADDOCK (it1) to refine the interfaces. The simplest form of this protocol, *protocol 1*, includes a simulated annealing step in which no additional restraints are provided to guide the refinement, followed by a final energy minimization in itw. For *protocol 2*, intermolecular Cα-Cα atom distances between residues at the PPI within an 8 Å cutoff are selected as restraints. To allow for movement of the individual chains, the upper distance limit is defined as the measured Cα-Cα distance padded with 1.5 Å. The lower bound distance was set to 0 Å. During refinement, 50% of the provided distance restraints is randomly excluded for each model generated. In *protocol 3*, ''ambiguous surface restraints'' are taken into account during it1. These are automatically calculated by HADDOCK as one ambiguous distance restraint per pair of components, defined between all Cα atoms of the two components with sum averaging and an upper limit of 7 Å. This restraint effectively enforces the two molecules to remain in contact while allowing for possible changes in the interfaces. The final restraints tested with the simulated annealing protocol are center of mass (CM) and centroid restraints in protocols 4 and 5, respectively. The center-of-mass restraints are automatically defined by HADDOCK between each pair of components as a distance restraint between the geometric center of the Cα atoms of the two components (center averaging). The upper distance limit for the restraints is the sum of the ''effective radius'' of each molecule, which is defined as half the average length of the two smallest principal components. Centroid restraints are distance restraints that effectively restrain the position of the geometric center of each component based on its Cα atoms to its original position.

Refinement in explicit water (protocol 6)

Besides protocols based on the it1 semi-flexible refinement, we have also tested the final refinement stage in explicit solvent (itw) as a stand-alone protocol (i.e. bypassing the it0 and it1 stage). In this setup (*protocol 6*), we used the experimental structure of the protein complex as a starting structure for itw. A solvent shell is built around the complex and, subsequently, a series of short MD simulations are performed using an integration time step of 2 fs: First, the system is heated to 300 K (500 MD steps at 100, 200 and 300 K) while all atoms except the side-chain atoms at the interface are restrained to their original position (force constant 5 kcal mol^{-1}). Next, 1250 MD steps are performed at 300 K with position restraints (force constant 1 kcal mol^{-1}) for heavy atoms which are not part of the PPI (residues not involved in intermolecular contacts within 5 Å). Finally, the system is cooled down (1000 MD steps at 300, 200 and 100 K) with position restraints on the backbone atoms of the protein complex, excluding the interface atoms (Dominguez et al., 2003; Van Zundert et al., 2016).

Refinement by coarse graining (protocols 7 and 8)

The most recent update of HADDOCK supports coarse graining (CG) (Honorato et al., 2019; Roel-Touris et al., 2019) in which models can be coarse grained using the Martini force field (Monticelli et al., 2008) to reduce computational time as well as to smoothen the energy landscape. The last step of the CG docking protocol in HADDOCK is the rebuilding of an all-atom (AA) model of the complex. This final CG-to-AA conversion step can also be used as a refinement protocol to remove intermolecular clashes as recently demonstrated in a membrane complexes docking protocol combining rigid-body docking with Lightdock (Jiménez-García et al., 2018) and refinement in HADDOCK (Roel-Touris et al., 2020). CG-to-AA conversion is achieved by defining distance restraints between the atomic particles and the CG particle of which they are a part of. Using these distance restraints, the initial atomistic models are fitted onto the CG representation and the interfaces are optimized (for details see Roel-Touris et al., 2019).

For this protocol, we first converted the reference structures to coarse-grained models and generated the CG-to-AA restraints (automatically done on the web server). Then, it0 and it1 were disabled and only itw was used, which includes the CG-to-AA conversion. The tested CG protocols included the CG-to-AA conversion and a final energy minimization for protocol 7 or CG-to-AA conversion with a final MD refinement in explicit solvent (as done for protocol 6) for protocol 8.

QUANTIFICATION AND STATISTICAL ANALYSIS

The performance of each protocol using the top 4 models of each complex according to their default itw HADDOCK score was assessed by analysing the intermolecular atomic clashes (i), the interface quality (ii), the cross-correlation with the cryo-EM density (iii), the overall structural quality (iv) and the secondary structure content (v). The first property we examined was the removal of atomic interface clashes (i) with respect to the reference structures. Atomic clashes in the protein complexes were calculated as intermolecular heavy atom contacts <2.5 Å. The quality of the interface (ii) based on the contacts between chains was evaluated by using Probe (Word et al., 1999) in default mode. Calculated probe scores were normalized according to the surface area ($Å^2$). The recently introduced PI score was used as a second method to assess the interface quality (Malhotra et al., 2021). This method uses a support vector machine model trained on 12 interface features calculated from the atomic complex models to score each interface. Individual PI scores are calculated for each interface within a model. For the analysis, the average PI score over the included PPIs was calculated for each model.

Besides the PPI quality, we also analyzed the overlap between the experimental electron density map (EDM) and the models. For this the cross-correlation (iii) of each model with its experimental EDM was obtained by using the Chimera *fit in map* function (Pettersen et al., 2004). First, a density map of the atomic refined model was generated by describing each atom as a Gaussian distribution with a width proportional to the resolution of the experimental map and an amplitude proportional to the atomic number. Subsequently, the maps were fitted iteratively (2000 steps), sampling over the three rotational and three translational axes until the overlap converged. The correlation was then calculated using Equation 1, where u represents grid point values of the generated map and v the trilinear interpolated point values of the experimental map.

$$Correlation = \frac{(u, v)}{|u||v|} \quad \text{(Equation 1)}$$

The overall structural quality (iv) of the models was checked by calculating the Ramachandran and rotamer outliers as well as the Molprobity score of the whole complex via Molprobity (Davis et al., 2007; Hintze et al., 2016; Williams et al., 2018). Additionally, Cα-atom geometries were analyzed by CaBLAM (Prisant et al., 2020). Finally, we calculated the percentage of secondary structure elements (v) of the protein complexes using STRIDE (Frishman and Argos, 1995) and compared the starting reference structures to determine the loss or gain in secondary structure.

Visualization of the complexes and preparation of the figures was performed using PyMOL (Schrodinger, 2015).